AMERICAN SOCIETY FOR MICROBIOLOGY | Antimicrobial Agents and Chemotherapy®

MECHANISMS OF RESISTANCE

β-Lactamase of *Mycobacterium tuberculosis* Shows Dynamics in the Active Site That Increase upon Inhibitor Binding

Wouter Elings,[a] Anamika Gaur,[a]* Anneloes J. Blok,[a] Monika Timmer,[a] Hugo van Ingen,[a]* Marcellus Ubbink[a]

[a]Leiden Institute of Chemistry, Leiden University, Leiden, The Netherlands

ABSTRACT The *Mycobacterium tuberculosis* β-lactamase BlaC is a broad-spectrum β-lactamase that can convert a range of β-lactam antibiotics. Enzymes with low specificity are expected to exhibit active-site flexibility. To probe the motions in BlaC, we studied the dynamic behavior in solution using nuclear magnetic resonance (NMR) spectroscopy. ^{15}N relaxation experiments show that BlaC is mostly rigid on the pico- to nanosecond timescale. Saturation transfer experiments indicate that also on the high-millisecond timescale BlaC is not dynamic. Using relaxation dispersion experiments, clear evidence was obtained for dynamics in the low-millisecond range, with an exchange rate of ca. 860 s^{-1}. The dynamic amide groups are localized in the active site. Upon formation of an adduct with the inhibitor avibactam, extensive line broadening occurs, indicating an increase in magnitude of the active-site dynamics. Furthermore, the rate of the motions increases significantly. Upon reaction with the inhibitor clavulanic acid, similar line broadening is accompanied by duplication of NMR signals, indicative of at least one additional, slower exchange process (exchange rate, k_{ex}, of $<$100 s^{-1}), while for this inhibitor also loss of pico- to nanosecond timescale rigidity is observed for some amides in the α domain. Possible sources of the observed dynamics, such as motions in the omega loop and rearrangements of active-site residues, are discussed. The increase in dynamics upon ligand binding argues against a model of inhibitor binding through conformational selection. Rather, the induced dynamics may serve to maximize the likelihood of sampling the optimal conformation for hydrolysis of the bound ligand.

KEYWORDS BlaC, clavulanic acid, avibactam, NMR spectroscopy, inhibition, chemical exchange, beta-lactamases, structural biology

A central question in chemical biology is how enzymes can have broad specificity. Enzyme catalysis depends on efficient binding of the substrate to the enzyme and on the precise positioning of active-site residues to stabilize the transition state. Substrates that are structurally diverse may require different active-site conformations to efficiently bind the substrates and stabilize their respective transition states (1–10). Consequently, a trade-off between active-site rigidity for precise positioning of amino acid side chains and flexibility for adaptation to various substrates will exist, requiring motions of parts of the enzyme. Protein motions can occur on a broad range of timescales. It has been hypothesized that enzymes that combine high catalytic efficiency with broad specificity do so by combining high rigidity on short timescales with flexibility on longer timescales (11). The dynamic behavior of Ambler class A β-lactamases TEM-1 and PSE-4 is in line with this idea (11–16). A combination of nuclear magnetic resonance (NMR) backbone dynamics studies and molecular dynamics (MD) simulations has revealed that these proteins are extraordinarily rigid on the pico- to nanosecond timescale and display microsecond to millisecond timescale motions in the vicinity of the active site, in particular in the Ω loop that encloses it on one side (Fig. 1). Dynamics experiments on proposed β-lactamase ancestors (17–19) and chimeric

Citation Elings W, Gaur A, Blok AJ, Timmer M, van Ingen H, Ubbink M. 2020. β-Lactamase of *Mycobacterium tuberculosis* shows dynamics in the active site that increase upon inhibitor binding. Antimicrob Agents Chemother 64:e02025-19. https://doi.org/10.1128/AAC.02025-19.

Address correspondence to Marcellus Ubbink, m.ubbink@chem.leidenuniv.nl.

* Present address: Anamika Gaur and Hugo van Ingen, Bijvoet Center for Biomolecular Research, Utrecht University, Utrecht, The Netherlands.

Received 9 October 2019
Returned for modification 23 October 2019
Accepted 19 December 2019
Accepted manuscript posted online 23 December 2019
Published 21 February 2020

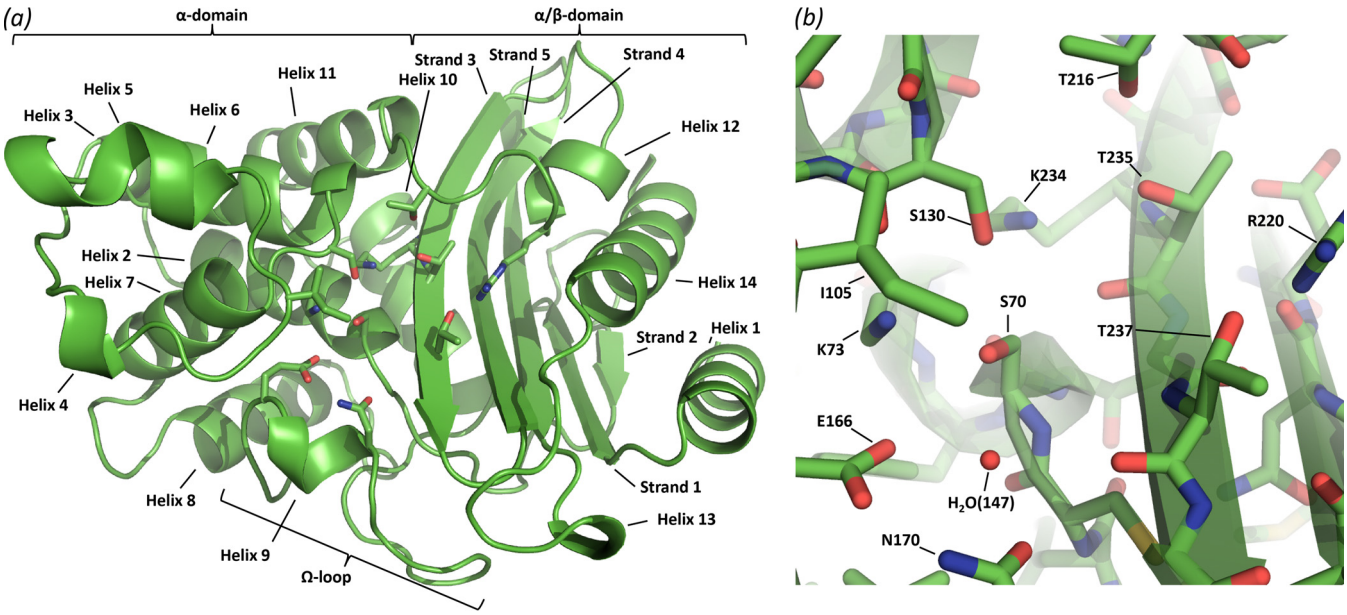

FIG 1 Crystal structure of BlaC (subunit A of PDB code 5NJ2) (31). (a) Cartoon representation with indication of α-helices, β-strands, and the Ω loop. Several active-site residues are shown in stick representation. (b) Detail of the active site, showing both a stick representation and transparent cartoon representation for clarity. Several active-site residues and the conserved active-site water molecule are indicated.

proteins (20, 21) suggested that this pattern of dynamics is a conserved feature. However, significant dynamic differences were found for individual residues, emphasizing the importance of comparing various β-lactamases (15, 22). The leading structural model to explain the active-site dynamics is slow motion of the Ω loop into and out of the active site. This loop contains residue Glu166, which acts as a general base for deacylation, activating a conserved water molecule for nucleophilic attack of the Ser70-bound carbonyl, which leads to hydrolysis of the bond between enzyme and adduct. Glu166 is also thought to play a similar role in acylation although Lys73 has alternatively been proposed as general base for this step (23, 24). Furthermore, other residues in the Ω loop, such as Asn170, also contribute favorable enzyme-substrate interactions. These interactions may require slightly different enzyme conformations with various substrates. If active-site flexibility is indeed required for adaptation to various substrates, it can be hypothesized that ligand binding will lock the active site in one conformation and thus freeze out the dynamics. NMR dynamics studies on β-lactamase/ligand complexes have not been reported to date although the potential relevance of insight into the bound-state dynamics has been recognized for years (15). The absence of such data may be due to technical difficulties as the typical length of NMR dynamics experiments is several days, restricting such studies to extremely stable complexes. Clearly, monitoring the dynamics during normal catalysis of substrates in this way is not feasible. However, β-lactamases do form stable covalent complexes with inhibitors. Inhibition of β-lactamases has clinical application (25–27) and is gaining in relevance with the increased prevalence of antibiotic resistance (28–30). In addition to this inherent interest in β-lactamase inhibition, inhibitor-bound β-lactamases may also serve as mimics of the covalent β-lactamase substrate complex during catalysis. We recently characterized the timescale of interaction between the β-lactamase of *Mycobacterium tuberculosis*, BlaC (Fig. 1), and the inhibitor clavulanic acid in different buffers (31). The high stability of the complex in morpholineethanesulfonic acid (MES) buffer opens up a window for NMR dynamics measurements. Also, the effects of the inhibitor avibactam, which binds reversibly rather than being degraded (32), can be measured using these techniques.

Here, we present the dynamic properties of BlaC and the first characterization of β-lactamase/inhibitor complex dynamics. The dynamic behavior of resting-state BlaC in

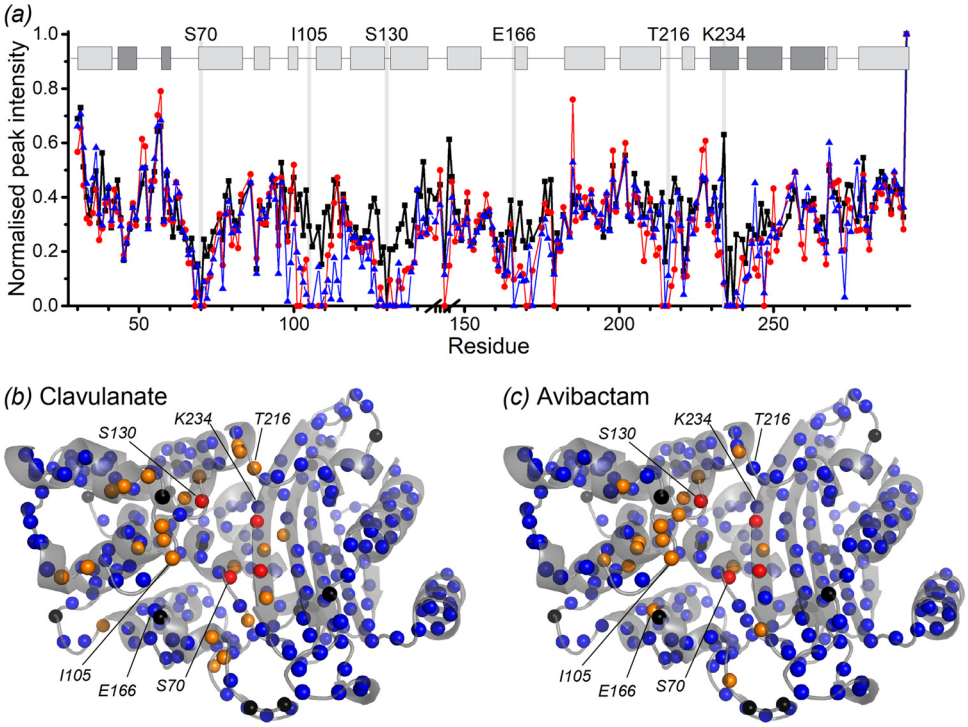

FIG 2 Peak intensities. (a) Relative peak intensities of assigned backbone amides in a ^{1}H-^{15}N TROSY spectrum for BlaC in the resting state (black squares), bound to clavulanic acid (red circles), and bound to avibactam (blue triangles). The resonance of the C-terminal amide was used for normalization. The break on the horizontal axis represents a BlaC-specific G-G-G-T loop which is not present in the Ambler numbering. Several active-site residues are indicated with gray bars. Secondary structure is indicated above the graph; light and dark gray boxes represent α-helices and β-strands, respectively. Error bars have been omitted for clarity; propagated error from the spectral noise is in all cases $<$0.03. (b and c) Visualization of binding effects on BlaC crystal structure with PDB code 5NJ2. Nonproline backbone amides for which no resonance was found in free BlaC are indicated with red spheres. Amides for which the resonance was lost upon inhibitor binding are indicated with orange spheres for clavulanic acid and avibactam, as indicated. Amides for which a resonance could be assigned for resting-state as well as bound BlaC are indicated with blue spheres. Proline nitrogen atoms are indicated with black spheres. Amides of several active-site residues are indicated for reference.

solution is very similar to that of other class A β-lactamases, and the rate of the active-site exchange process is ca. 860 s^{-1} at 298 K. The high rigidity, which is a hallmark of β-lactamases, is locally lost upon inhibition by clavulanic acid. Furthermore, upon binding to either clavulanic acid or avibactam, the effects of chemical exchange in the active site become more extensive, clearly showing that inhibitor binding does not lock the active site in one conformation.

RESULTS

Resting-state BlaC. The ^{1}H-^{15}N correlation spectra of BlaC are well dispersed (see Fig. S1 in the supplemental material). The backbone amide assignment of resting-state BlaC without tag was derived from the previously published assignment of the tagged protein (31) via comparison with an HNCA spectrum. In this way, 98% of the resonances of the BlaC backbone H-N moieties could be assigned. As with the tagged protein, the four residues at hydrogen-bonding distance from the active-site phosphate were the only nonproline, nonterminal residues for which backbone resonances could not be found. The four missing resonances, as well as the lower peak intensities of the surrounding amides (Fig. 2a, black squares), suggest that an intermediate to fast exchange process may be present in the active site.

To characterize the dynamics processes, the ^{15}N longitudinal relaxation time (T_1), ^{15}N transverse relaxation time (T_2) and the ^{15}N-{^{1}H} nuclear Overhauser effect (NOE) of the BlaC backbone amides were measured at two magnetic fields, 14 T and 20 T (Fig. S2 and S3). The obtained NOE ratios show lower values for loop and surface regions of

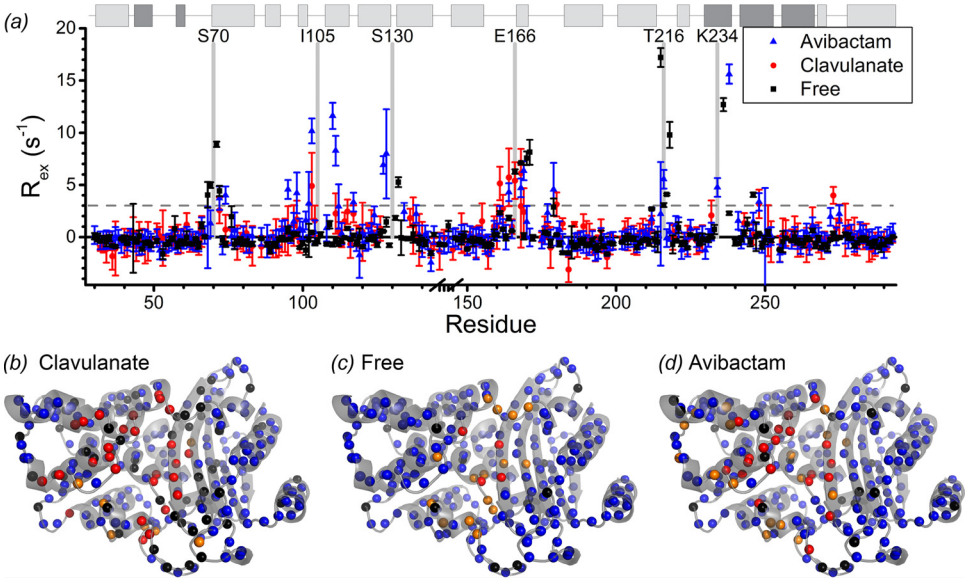

FIG 3 CPMG relaxation dispersion data. (a) Contribution of chemical exchange to the R_2 relaxation of backbone ^{15}N resonances in BlaC resting state (black), bound to clavulanic acid (red), and bound to avibactam (blue), as measured by CPMG relaxation dispersion analysis at 20 T. R_{ex} is defined as the $R_{2,eff}$ at ν_{CPMG} = 25 s^{-1} minus that at 1,000 s^{-1}. Error bars represent the 95% confidence interval based on three duplicate delays per experiment. The break on the horizontal axis represents a BlaC-specific G-G-G-T loop which is not present in the Ambler numbering. Several active-site residues are indicated with gray bars. Secondary structure is indicated above the graph; light and dark gray boxes represent α-helices and β-strands, respectively. (b to d) Visualization of millisecond dynamics on BlaC of PDB structure 5NJ2 (31) for BlaC bound to clavulanic acid, in a free state, and bound to avibactam, as indicated. Backbone amides for which R_{ex} values are <3 s^{-1} are displayed as blue spheres, and those with R_{ex} value of >3 s^{-1} are shown as orange spheres. Residues whose resonances were broadened beyond detection are displayed as red spheres, while those for which R_{ex} could not be determined for another reason (e.g., prolines or too much peak overlap) are displayed as black spheres.

the protein as well as an unexpectedly low ratio for Val80 (Fig. S2), but, overall, BlaC is clearly a rigid protein on the pico- to nanosecond timescale. Lipari-Szabo model-free analysis of the two-field T_1, T_2, and NOE data was performed using an anisotropic diffusion tensor, yielding an average rotational correlation time of 13.81 $\pm$ 0.04 ns. This is close to an estimate using HydroNMR (33) and the crystal structure of PDB code 5NJ2 (31) (14.5 ns). Fitting of the spectral densities resulted in an average order parameter over 0.9 and yielded very few dynamic regions, confirming that BlaC is rigid on the short timescales (Fig. S4). Most amides were best fitted with anisotropic models 1 to 4 (see Materials and Methods). Model 5, including an extra local-order parameter S_f^2 for very fast motion, was used to fit only the data for Val80. The resulting order parameters are S_f^2 = 0.79 $\pm$ 0.03 and S^2 = 0.57 $\pm$ 0.02, the latter of which is the lowest order parameter in the protein. The other regions that exhibit some flexibility correspond with elements that are expected to be flexible based on the structure, such as the loop between β-strands 1 and 2 and that between α-helices 7 and 8.

Several residues could not be modeled without the inclusion of a chemical exchange parameter, so the possibility of exchange on the millisecond timescale was examined using Carr-Purcell-Meiboom-Gill (CPMG) relaxation dispersion measurements at magnetic field strengths of 14 T and 20 T. Dispersion of relaxation rates over the CPMG pulse frequency, indicating millisecond chemical exchange, was observed centered clearly around the active site (Fig. 3a and c, orange spheres).

Eight active-site residues that showed similar dispersion profiles at both magnetic field strengths were used in a group fit (Fig. 4 and Fig. S5), yielding a chemical exchange rate of (8.6 $\pm$ 0.6) $\times$ 10^2 s^{-1}. This exchange rate agrees with the (8.5 $\pm$ 2.1) $\times$ 10^2 s^{-1} that was found for TEM-1 with single-field relaxation dispersion (21). The excited-state population and chemical shift differences could not be determined with any accuracy.

To investigate the possibility of even slower dynamic processes, chemical exchange saturation transfer (CEST) in resting-state BlaC was also measured. Experiments with

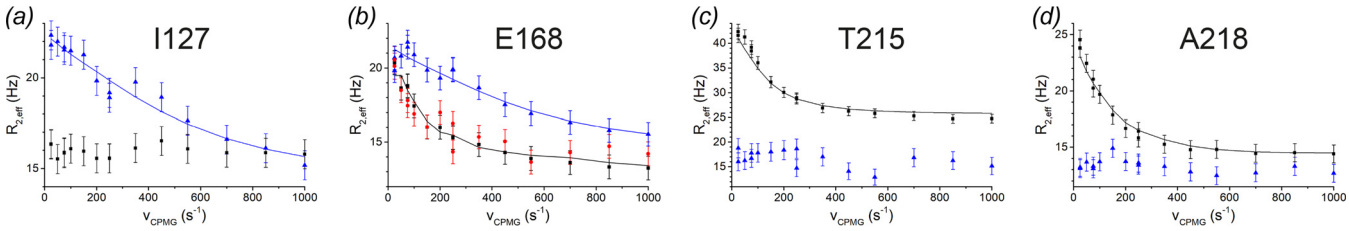

FIG 4 Example CPMG relaxation dispersion profiles, as measured for the backbone amide resonances of the indicated residues at 20 T. Data obtained in the free state, bound to clavulanic acid adduct, and bound to avibactam are represented in black squares, red circles, and blue triangles, respectively. Error bars represent the standard deviations based on three duplicate CPMG frequencies, with a user-defined minimum of 0.8 s^{-1} to avoid overfitting. Lines represent global fits to a two-state exchange model as described in the text.

saturation fields of 25 Hz and 8 Hz and at temperatures of 298 K and 288 K all failed to reveal chemical exchange for any of the residues, suggesting that no significant dynamics in the CEST timescale of 20 to 200 s^{-1} are present. An example profile is provided in Fig. S6.

Inhibitor-bound BlaC. The effect of BlaC inhibition on its dynamic behavior was studied by performing NMR experiments on 0.38 mM BlaC with 2 mM avibactam or 100 mM clavulanic acid. Avibactam is not hydrolyzed by BlaC, as was observed by other investigators (32, 34) and also in our experiments (data not shown). Clavulanate has an ~1.2-h turnover time under these conditions (31), so this large excess of clavulanic acid allowed the recording of multidimensional NMR experiments on the BlaC-inhibitor complex. This turnover rate is much too low to affect the employed NMR dynamics experiments. Furthermore, the rate is much lower than that of the other catalytic steps, so the adduct accumulates to a fraction close to 100%. Previously, this major species was shown by mass spectrometry to be a 70-Da covalent adduct (31). Thus, the NMR dynamics measurements report on conformational dynamics of this major species. The ^{1}H-^{15}N transverse relaxation-optimized heteronuclear single quantum coherence (TROSY-HSQC) spectra of backbone amides of BlaC bound to each inhibitor were assigned by comparison to the spectra of resting-state BlaC, with additional help of HNCA spectra of ^{15}N-^{13}C-labeled BlaC-inhibitor samples to confirm the assignments.

Avibactam. Avibactam was titrated into a BlaC sample, and ^{1}H-^{15}N TROSY-HSQCs were recorded at various avibactam concentrations, showing chemical shift perturbations of the BlaC backbone amide resonances in the slow-exchange regime. Line shapes for the resonances of six amides were fitted with a two-state binding model using TITAN software (35), yielding upper limits for the apparent equilibrium dissociation constant (K_D) and off-rate constant, k_{off}, of 10 μM and 10 s^{-1}, respectively (Fig. S7). This apparent k_{off} is in line with the 1×10^{-2} s^{-1} found by Soroka et al. (32), while the apparent K_D indicates that the low efficacy of BlaC inhibition by avibactam is caused by the very low on-rate rather than by low affinity. Interestingly, several peaks that are visible in the spectrum of resting-state BlaC broaden beyond detection upon binding with avibactam (Fig. 2). These peaks correspond to amides around the binding site, indicating that inhibitor binding induces enhanced chemical exchange broadening in the active site. T_1, T_2, and NOE experiments performed at 20 T (Fig. S8 and S9) show little change in dynamic behavior relative to that of the resting state, other than decreased transverse relaxation times around the loop containing Ile105. As with the exchange broadening, this hints at induction of a slow or intermediate exchange process. The unexpectedly high transverse relaxation time and low NOE for Val80 were not found in the avibactam-bound state.

CPMG relaxation dispersion measurements at 20 T showed an increased magnitude of the exchange relaxation (R_{ex}) in the loops of the α domain around the residues whose resonances broadened beyond detection (Fig. 3). The exchange profiles of the individual residues over the pulse frequency are visibly different from those in the free state (Fig. 4 and Fig. S10), indicating a significantly faster exchange process than the 860 s^{-1} that was found for the resting state. A single-field global fit of the exchange

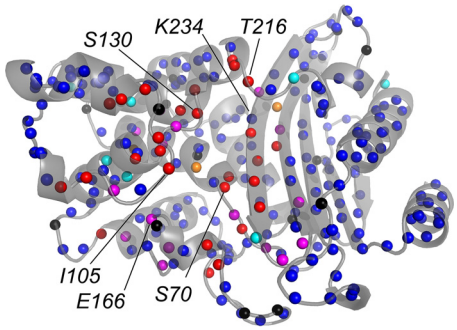

FIG 5 Dynamics of BlaC upon reaction with clavulanic acid. Backbone amides for which the resonance has broadened beyond detection are displayed in red, those for which multiple resonances could be assigned are shown in magenta, those for which a transverse relaxation time T_2 of >60 ms was found are shown in cyan, those for which the cyan and magenta conditions are both true are shown in orange, and those for which no severe dynamics were detected are shown in blue. Proline nitrogen atoms are displayed in black.

profiles of 19 backbone amides (Fig. S10) yielded an estimate of the active-site exchange rate in the avibactam-bound state of $(3.4 \pm 0.2) \times 10^3$ s^{-1}. The exchange between free and avibactam-bound BlaC is very slow ($\ll$100 s^{-1}), so the chemical exchange process measured here occurs in the bound state. The enhanced exchange effects are observed around the binding site, particularly in the loops containing Ser130 and Ile105.

Clavulanic acid. Upon binding with clavulanic acid, as with avibactam, the resonances of several amides around the binding site broadened beyond detection (Fig. 2). Moreover, in the clavulanic acid adduct-bound state, at least 21 resonances were found to split into two or more distinct peaks of similar intensities. These peaks belong to amides around the active site and in the α domain (Fig. 5, magenta and orange spheres). Furthermore, the clavulanic acid adduct-bound state of BlaC is less stable over time than the free and avibactam-bound states. Over the course of days, a gradual appearance of broad background signal in the center of the spectrum was observed, suggesting the formation of a molten globule.

The T_1, T_2, and NOE of clavulanate-bound BlaC were measured at 20 T (Fig. S8 and S9). Average relaxation times (T_1 and T_2, respectively) were found to have shifted from 1.7 s and 45 ms for resting-state BlaC to 1.8 s and 40 ms for the adduct, which may be caused by an increase in sample viscosity due to the addition of 100 mM clavulanic acid. Strikingly higher transverse relaxation times were found for several residues in and near loops and terminal regions, as well as for six residues involved in the hydrophobic packing interface between helices 2 and 7 in the α subunit. Moreover, for these residues, the NOE is lower than that in resting-state BlaC. These observations indicate a severe local decrease of internal rigidity upon clavulanic acid inhibition, particularly in loop regions and on the interface between helices 2 and 7.

CPMG relaxation dispersion measurements at 20 T were also performed on clavulanate-bound BlaC. However, most of the resonances that show exchange broadening in the resting-state protein were broadened beyond detection in the clavulanate-bound spectra. Moreover, due to the splitting of peaks and the gradual appearance of molten globule-like background signal over time, accurate line shape fitting of the resonances proved impossible in many cases. Residues Glu168 and Asp273 were found to have dispersion profiles with shapes similar to those in the active-site exchange of the resting-state protein (e.g., Fig. 4b). Slight elevations in the R_{ex} are observed around the loop containing Ile105, near the base of the Ω loop, and for residue Asp273, but overall the profile of exchange relaxation over all residues, keeping in mind the larger error and the missing data, looks rather similar to that of resting-state BlaC (Fig. 3). Thus, it seems that the resting-state BlaC dynamics are still present upon formation of the clavulanic acid adduct and that at the same time additional states are being populated, causing line broadening and peak splitting.

DISCUSSION

We show that resting-state BlaC is mostly rigid on the pico- to nanosecond timescale, which is similar to the behavior of the other class A β-lactamases for which NMR dynamics studies have been performed, TEM-1 (11, 13, 14) and PSE-4 (15). Only Val80 was found to exhibit fast motion, as modeled from the low NOE ratios and elevated T_2 relaxation times for its backbone amide. This is surprising as this amide is located in the long α-helix 2, and the Val80 side chain does not face the outside of the protein but, rather, the interface between helices 2 and 7.

The BlaC active site exhibits flexibility on the millisecond timescale, as observed by both CPMG relaxation dispersion studies and the broadening beyond detection of several important active-site residues (Ser70, Ser130, Thr235, and Thr237). This behavior is also similar to that of other class A β-lactamases (11–20), and the localization of this chemical exchange in the active site suggests that the dynamics may play a role in catalysis. This can only be the case if the dynamics are as fast as or faster than the maximum catalytic turnover rate of the enzyme. The observed exchange rate of $(8.6 \pm 0.6) \times 10^2$ s^{-1}, obtained under the assumption of a two-state exchange model, is higher than the fastest k_{cat} that was reported for BlaC, 111 ± 4 s^{-1} for nitrocefin hydrolysis (36), which implies that enzyme dynamics may be relevant for catalysis. On the basis of the Bloch-McConnell equations for chemical exchange, it can be shown that at an exchange rate of 860 s^{-1}, the population of the minor state must be sizeable (>15%) for the resonances of Ser70, Ser130, Thr235, and Thr237 to broaden beyond detection at 20 T. The chemical shift difference between the major and minor state must be larger than 0.1 ppm for ^{1}H and/or 1 ppm for ^{15}N. The link between these four residues is that in every BlaC crystal structure published to date, their respective side chains each contribute to the hydrogen bonding with either the carboxyl group of a ligand or a phosphate or acetate ion from the buffer. However, upon titration with phosphate, the resonances do not appear (31), meaning that the binding and dissociation of phosphate cannot explain the chemical exchange broadening of these peaks.

We also report the first study of a class A β-lactamase dynamics upon inhibitor binding. On the pico- to nanosecond timescale, the reaction with avibactam stabilizes the Val80 amide while that with clavulanic acid leads to fast motions for various residues, notably including several that are involved in the hydrophobic packing interface between helices 2 and 7, similar to what was observed for Val80 in resting-state BlaC. This result resembles the observation by Stivers et al. that several residues of 4-oxalocrotonate tautomerase show a decrease in the order parameter upon inhibitor binding (37). The authors suggest that the increased flexibility of these residues serves as an entropic contribution to the overall free energy change upon binding, which may well be the same for BlaC. An increase in fast dynamics of backbone amides generally indicates increased flexibility of the peptide bond. Many of the amides for which we observed this phenomenon are on the interface of helices 2 and 7. An increase of backbone flexibility implies reduced stability of the hydrophobic core in that region of the α domain.

On the millisecond timescale, binding of BlaC to either avibactam or clavulanic acid leads to increased effects of dynamics. In the avibactam-bound state, we observed broadening beyond detection of some peaks and relaxation dispersion of others. All affected amides surround the active site. For the broadening beyond detection at 20 T to be caused by the ~3,400 s^{-1} exchange process identified using CPMG experiments, chemical shift differences between the two states that are larger than ca. 0.3 ppm for ^{1}H and/or 3 ppm for ^{15}N would be required. Alternatively, it is possible that multiple exchange processes take place in the same region of the protein. In any case, the relaxation dispersion results suggest that avibactam binding speeds up the active-site exchange process in BlaC significantly.

Inhibition of BlaC with clavulanic acid was likewise accompanied by broadening of many resonances in and around the active site of BlaC. These experiments were performed in the presence of a high initial concentration of clavulanic acid, so it cannot

be excluded entirely that noncovalent binding of an additional clavulanic acid molecule to the BlaC adduct could cause line broadening. However, an earlier study on such binding to a catalytically inactive mutant of BlaC (S70A) showed that if binding occurs at all, the affinity must be very low indeed, and line broadening in the BlaC NMR spectrum was not observed (38). Therefore, we attribute the increased dynamics to the adduct formation.

The chemical environment of all of the catalytic residues as well as residues in all of the nearby regions appears to be affected by the motions. Interestingly, β-lactam binding was previously reported to also cause increased millisecond dynamics in the active site of a LD-transpeptidase (39) as well as in that of a signal transducer β-lactam-sensing domain (40), suggesting that this behavior might be conserved across a wide range of β-lactam binding proteins.

The question arises as to how these relatively small adducts, especially the clavulanic acid adduct, which is a mere 70 Da (5 heavy atoms), can have such a major impact on such a broad region of the protein. Sagar et al. (41) reported small-angle X-ray scattering (SAXS) data yielding an unexpectedly large solvation radius for free BlaC in solution, while BlaC bound to clavulanic acid was found to have a solvation radius closer to that which is expected based on the crystal structure. The authors proposed that free BlaC in solution adopts an open conformation, whereas inhibitor binding locks BlaC in the closed conformation that has been observed in all crystal structures so far. If resting-state BlaC were, indeed, to adapt an open conformation in solution, it would likely exhibit a larger rotational correlation time and thus higher transverse and lower longitudinal relaxation times than in the canonical closed conformation. The correlation time measured for the free BlaC on the basis of the relaxation data matched the one calculated from the crystal structure. Binding avibactam did not change the relaxation times much, and the sample with clavulanic acid bound even yielded relaxation times indicating an increase of the correlation time. However, the latter was likely caused by an increase in sample viscosity due to the high concentration of the inhibitor. Summarizing, our data provide no evidence for an open state of resting-state BlaC. For related β-lactamases, it has been suggested (11, 15, 16) that the process underlying the chemical exchange effects is movement of the tip of the Ω loop into and out of the active site. Such movement could facilitate the flow of solvent and substrate and aid in positioning of the substrate in the active orientation. If so, the motion would likely affect amides in all regions that are in contact with the tip of the Ω loop, such as helix 7 and the loops containing Ser130 and Ile105. This model thus fits well with our data.

To gain more insight into what the various states may look like structurally, we compared bound and unbound β-lactamase crystal structures. Most structures showed little variation between bound and unbound forms. In the structure of PDB code 6H2H (38) BlaC bound to avibactam, however, the Ω loop was observed in a slightly open conformation, with the Cα atoms of Asn170 and Arg171 positioned $\sim$2 Å further away from the active site than their canonical positions, providing further support for the model of Ω-loop movement (Fig. 6). Our data suggest the presence of multiple dynamic processes in the bound state. Recently, Olmos et al. (42) reported an X-ray free-electron laser (XFEL) study with snapshots at 30, 100, 500, and 2,000 ms of the catalytic reaction of ceftriaxone hydrolysis by BlaC. The structures obtained during the reaction show almost no structural variation compared to that of BlaC in the resting state. The only active-site residues of which the orientation varies between the structures are Lys73 and Ser130. The Lys73 orientations are similar to those reported by Vandavasi et al. for class A β-lactamase Toho-1 (24), except that the noncanonical conformation is oriented toward Ser130, whereas in BlaC it is oriented toward Glu166. One of these conformations allows an extra water molecule to penetrate deep into the active site, between helix 2 (Lys73) and helix 7 (Met135, which is an alanine in BlaC), suggesting a defect of the hydrophobic core such as that we observed upon clavulanic acid binding in BlaC. The occupancies of the observed states, 41 and 59%, respectively, also match the relative occupancies of the doubled peaks of 42% $\pm$ 3% that we observed in our clavulanic acid adduct-bound-state spectra. An increasing body of evidence suggests

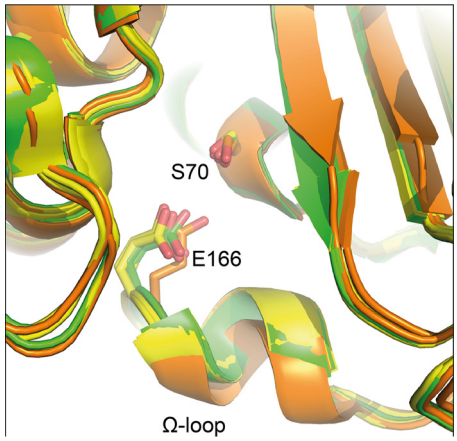

FIG 6 Ω-Loop displacement model. Cartoon representations of the BlaC active site in a superposition of BlaC crystal structures in free form (PDB codes 5NJ2 and 5OYO) (31) are shown in green, those bound to clavulanic acid adduct (PDB codes 3CG5 [61], 6H2C, and 6H2G [38]) are shown in yellow, and those bound to avibactam (PDB codes 4DF6 [34] and 6H2H [38]) are shown in orange. Active-site residues Ser70 and Glu166 are shown in stick representation; adducts are omitted for clarity. The structure of BlaC of PDB code 6H2H bound to avibactam displays a more open conformation of the Ω loop.

that Lys73 can act as a general base for catalysis (24, 43–46). Langan et al. even found that in Toho-1 β-lactamase, Lys73 and several other active-site residues alter their conformations in reaction to substrate binding (47). It therefore seems possible that the chemical exchange we observed upon clavulanic acid binding is related to the interconversion of Lys73 between different conformations (Fig. 7). As has been suggested before (45, 47, 48), the Lys73 side chain may need to be in one conformation for efficient substrate binding and in another for efficient product release. Thus, it seems possible that the two conformations observed in the crystal structures of Toho-1 (24, 46–49) and BlaC (42) are the cause of the two forms that we observed in the NMR spectra of the BlaC-clavulanic acid adduct. In this way the effects of addition of the small adduct to Ser70 can be transmitted further into and around the active site.

In conclusion, we show that BlaC is highly rigid on the pico- to nanosecond timescale but exhibits flexibility on the millisecond time scale in and around the active site, with an exchange rate of ca. 860 s^{-1}. The dynamic behavior of free BlaC is very similar to that of the other class A β-lactamases for which dynamics studies were

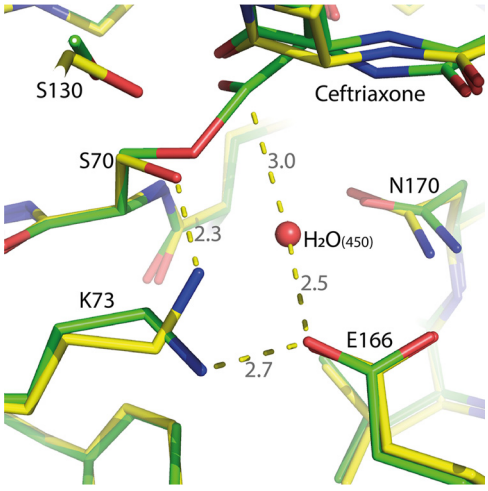

FIG 7 Model involving reorientation of Lys73. BlaC structures observed by Olmos et al. representing bound (PDB code 5A92; green carbons) and unbound (PDB code 5A91; yellow carbons) states show different orientations for the side chain of Lys73 (42). Indicated distances are in angstroms.

performed and therefore appears to be conserved among class A β-lactamases. We also show that upon inhibition with clavulanic acid, pico- to nanosecond stability of the hydrophobic core in the α-domain is disturbed. Moreover, upon binding of either clavulanic acid or avibactam, the prevalence of millisecond dynamics around the active site increases dramatically. In this work we studied the dynamics in BlaC-inhibitor complexes, so the question remains as to what effect this phenomenon has on the timescale of substrate catalysis. We hypothesized that active-site flexibility of β-lactamases represents exchange between respective binding modes for the various substrates. The observation that inhibitor binding does not lock the active site in one conformation but, rather, increases the dynamics argues against a model of inhibitor binding through conformational selection. Rather, the induced dynamics may serve to maximize the likelihood of sampling the precise conformation that lowers the hydrolysis transition state energy barrier for this substrate the most.

MATERIALS AND METHODS

Materials. Pure BlaC without signal peptide and a purification tag (sequence detailed in Fig. S11 in the supplemental material) was obtained as described previously (31). The Ambler standard β-lactamase numbering scheme (Fig. S11) is used throughout this text (50). Clavulanic acid from the manufacturer Matrix Scientific was used, and concentrations were determined using the previously determined extinction coefficient at 256 nm of 20.0 (0.1) $mM^{-1}\,cm^{-1}$ (31). Avibactam was used from the manufacturer MedChem Express, and concentration was determined using one-dimensional (1D) ^{1}H quantitative NMR with trimethylsilyl propionate (TSP) as a known standard.

Methods. Unless mentioned otherwise, all experiments were performed on samples containing 0.38 mM ^{15}N-enriched BlaC in 94 mM MES-NaOH, pH 6.4, and 6% D_2O at 298 K. Measurements of inhibitor-bound BlaC were performed on samples obtained by mixing BlaC with the inhibitor in the same buffer to obtain concentrations after mixing of 0.38 mM BlaC and either 100 mM clavulanic acid or 2 mM avibactam, unless mentioned otherwise. NMR spectra were recorded on a Bruker AVIII HD 850 MHz (20 T) or Bruker AVIII 600 MHz (14 T) spectrometer equipped with a TCI CryoProbe or a TXI probe, respectively. ^{1}H-^{15}N transverse relaxation optimized heteronuclear single quantum coherence (TROSY-HSQC) (51, 52) spectra were recorded and assigned using HNCA spectra on samples containing 0.7, 0.4, or 0.3 mM ^{15}N-^{13}C-enriched BlaC without inhibitor, with 186 mM clavulanic acid, or with 2 mM avibactam, respectively, in the same buffer. These spectra were recorded using the standard Bruker pulse program trhncaetgp3d, processed with Topspin, version 3.2 (Bruker BioSpin), and analyzed using CCPNmr analysis (53). Assignment was performed by comparison of the TROSY-HSQC and HNCA spectra with those of the previously assigned BlaC with a 6×His purification tag (Biological Magnetic Resonance Bank [BMRB] accession no. 27067) (31). Nuclear Overhauser effect (NOE) measurements were performed using the standard Bruker pulse program hsqcnoef3gpsi, with a ^{1}H saturation delay of 4 s. ^{15}N longitudinal relaxation time (T_1) measurements were performed using the standard Bruker pulse program hsqct1etf3gpsitc3d, with a recycle delay between experiments of 6 s and variable delays of 0.12, 0.17, 0.24 (2×), 0.33, 0.46, 0.65, 0.91, 1.28 (2×), 1.78, and 2.50 s. ^{15}N transverse relaxation time (T_2) measurements were performed using the standard Bruker pulse program hsqct2etf3gpsitc3d, with a recycle delay between experiments of 4 s and 500 Hz CPMG refocusing strength during variable T_2 delays of ca. 0, 17, 34 (2×), 51, 68, 85, 102, 119 (2×), 136, and 153 ms. All relaxation experiments were acquired in an interleaved manner. T_1 and T_2 data were processed with Topspin, version 3.2, and resulting peak heights were fitted to exponential decay curves using Dynamics Center, version 2.5 (Bruker BioSpin). NOE data were processed and analyzed with the same software.

Lipari-Szabo analysis was performed with Dynamics Center, version 2.5. Only residues for which the NOE is >0.75 and the T_1 and T_2 values were each within one standard deviation of their respective means were used to fit the diffusion tensor. The diffusion (D) was found to be anisotropic, with an average rotational correlation time, τ_c, of $1/[2 \times (D_{xx} + D_{yy} + D_{zz})]$ (54), in line with a prediction from subunit A of the crystal structure of PDB code 5NJ2, after deletion of the histidine tag and linker, using HydroNMR (33). Least-squares fitting of the reduced spectral density function, $j(\omega)$, to the relaxation parameters was performed with 1,000 iterations with random starting parameters, using an NH bond length of 1.02 Å and an average chemical shift anisotropy of −160 ppm. To avoid overfitting of relaxation parameters with small errors, Lipari-Szabo analyses were performed with user-defined errors of 10% (T_1) and 5% (T_2 and NOE) of the respective values. Relaxation data from each residue were fitted with the five standard models for internal motions, using anisotropic overall motion (55, 56). In model 1, the order parameter S^2 is fitted for each residue, while the correlation times, τ_j, are calculated from components and orientation of the diffusion tensor, which is a global parameter. In model 2, a local correlation time, τ_e, for fast motion is additionally fitted individually for each residue. Model 3 is the same as model 1, except that an R_{ex} term is added to the relaxion rate constant R_2 in the calculation of the reduced spectral densities. Likewise, model 4 is the same as model 2 with the addition of an R_{ex} term. In model 5, an extra modeling parameter, S_f^2, is included for very fast local motion. The best model was selected based on the lowest Akaike information criterion (AIC) value, which is the sum of the χ^2 of the fit and the number of

fitted parameters × 2. The selected model for each residue is reported with the relaxation data at BMRB (see above).

CPMG relaxation dispersion measurements were performed on 1.0, 0.8, or 0.4 mM ^{15}N-enriched BlaC samples for free protein at 20 T and at 14 T or with 100 mM inhibitor at 20 T, respectively. The TROSY CPMG pulse program as detailed by Vallurupalli et al. (57) was used, with two blocks of 1 (2×), 2, 3 (2×), 4, 6, 8, 10 (2×), 14, 18, 22, 28, 34, and 40 ^{15}N 180° pulses in a 40-ms relaxation time, respectively. The length of the CPMG refocusing pulse was 84 μs or 90 μs at 20 T or 14 T, respectively, and the carrier was set to the center of the spectrum at 119 ppm. Data were acquired in interleaved manner with a recycle delay of 2 s. Data were processed with NMRPipe (58), and resulting resonances were fitted to a glore line shape using FuDa (59). Effective transverse relaxation rates, $R_{2,\mathrm{eff}}$, were calculated from the fitted peak heights according to the following calculation: $R_{2,\mathrm{eff}}(\nu_{\mathrm{CPMG}}) = -\ln\,(I(\nu_{\mathrm{CPMG}})/I_0)/T_{\mathrm{ex}}$. In the relaxation dispersion data of BlaC bound to clavulanic acid, 29 of the 208 fitted profiles showed variations that were much bigger than the experimental noise level. This variation is likely due to technical imperfections, so these data points were excluded from further analysis. An exclusion cutoff of 10 s^{-1} total increase in $R_{2,\mathrm{eff}}$ between subsequent pulse frequencies was used. Chemical exchange rates were determined with a grouped fit with the software CATIA (60), using a minimum $R_{2,\mathrm{eff}}$ standard deviation of 0.8 s^{-1} to avoid overfitting.

Chemical exchange saturation transfer (CEST) measurements were performed on 0.8 mM [^{15}N]BlaC samples, using the standard Bruker hsqc_cest_etf3gpsitc3d pulse program, with a 2.5-s recycle delay and 0.8-s B_1 irradiation at 8 and 25 Hz at frequencies in the ^{15}N range 100.5:0.5:130 ppm.

Titration of BlaC with avibactam was performed by adding a solution of 6 mM avibactam in 94 mM MES-NaOH, pH 6.4, and 6% D_2O to a sample of 0.27 mM ^{15}N-enriched BlaC in the same buffer to obtain concentrations of 0, 0.02, 0.07, 0.1, 0.2, 0.3, 0.4, 0.6, 0.7, and 0.9 mM avibactam. The final protein concentration was 0.23 mM. Affinity and off-rate were determined by fitting the peak shapes of Cys69, Arg161, Leu162, Glu168, Tyr241, and Ala274 over the course of the titration to a two-state binding model in TITAN (35). The resulting standard deviations of the fitted K_D and k_{off} were unrealistically small, even after bootstrapping with 100 replicas, so the values are reported as an estimated confidence interval based on systematic variation of the parameters (Fig. S7).

Figures containing the protein structure were created using the PyMOL Molecular Graphics System, version 2.2 (Schrödinger, LLC).

Data availability. NMR chemical shift assignments and relaxation data have been submitted to the BMRB and can be accessed under BMRB accession numbers 27888 (free state) (http://www.bmrb.wisc.edu/data_library/summary/index.php?bmrbId=27888), 27890 (clavulanic acid adduct-bound state) (http://www.bmrb.wisc.edu/data_library/summary/index.php?bmrbId=27890), and 27929 (avibactam-bound state) (http://www.bmrb.wisc.edu/data_library/summary/index.php?bmrbId=27929).

SUPPLEMENTAL MATERIAL

Supplemental material is available online only.

SUPPLEMENTAL FILE 1, PDF file, 2.1 MB.

ACKNOWLEDGMENTS

We thank Karthick Sai Sankar Gupta and Alfons Lefeber for their assistance with the NMR spectrometers and Lewis Kay for providing the TROSY-CPMG pulse sequence.

This study was supported by internal funding and by grant number 723.013.010 from the Netherlands Organization for Scientific Research.

We have no competing financial interests to declare.

REFERENCES

1. Greives N, Zhou H-X. 2014. Both protein dynamics and ligand concentration can shift the binding mechanism between conformational selection and induced fit. Proc Natl Acad Sci U S A 111:10197–10202. https://doi.org/10.1073/pnas.1407545111.
2. Vogt AD, Di Cera E. 2012. Conformational selection or induced fit? A critical appraisal of the kinetic mechanism. Biochemistry 51:5894–5902. https://doi.org/10.1021/bi3006913.
3. Du X, Li Y, Xia Y-L, Ai S-M, Liang J, Sang P, Ji X-L, Liu S-Q. 2016. Insights into protein-ligand interactions: mechanisms, models, and methods. Int J Mol Sci 17:E144. https://doi.org/10.3390/ijms17020144.
4. Yon JM, Perahia D, Ghélis C. 1998. Conformational dynamics and enzyme activity. Biochimie 80:33–42. https://doi.org/10.1016/s0300-9084(98)80054-0.
5. Wand AJ. 2001. Dynamic activation of protein function: a view emerging from NMR spectroscopy. Nat Struct Biol 8:926–931. https://doi.org/10.1038/nsb1101-926.
6. Kay LE. 2005. NMR studies of protein structure and dynamics. J Magn Reson 173:193–207. https://doi.org/10.1016/j.jmr.2004.11.021.
7. Bhabha G, Lee J, Ekiert DC, Gam J, Wilson IA, Dyson HJ, Benkovic SJ, Wright PE. 2011. A dynamic knockout reveals that conformational fluctuations influence the chemical step of enzyme catalysis. Science 332:234–238. https://doi.org/10.1126/science.1198542.
8. Kohen A. 2015. Role of dynamics in enzyme catalysis: substantial versus semantic controversies. Acc Chem Res 48:466–473. https://doi.org/10.1021/ar500322s.
9. Kovermann M, Rogne P, Wolf-Watz M. 2016. Protein dynamics and function from solution state NMR spectroscopy. Q Rev Biophys 49:e6. https://doi.org/10.1017/S0033583516000019.
10. Petrović D, Risso VA, Kamerlin SCL, Sanchez-Ruiz JM. 2018. Conformational dynamics and enzyme evolution. J R Soc Interface 15:20180330. https://doi.org/10.1098/rsif.2018.0330.
11. Fisette O, Morin S, Savard P-Y, Lagüe P, Gagné SM. 2010. TEM-1 backbone dynamics-insights from combined molecular dynamics and nuclear magnetic resonance. Biophys J 98:637–645. https://doi.org/10.1016/j.bpj.2009.08.061.
12. Roccatano D, Sbardella G, Aschi M, Amicosante G, Bossa C, Di Nola A, Mazza F. 2005. Dynamical aspects of TEM-1 β-lactamase probed by molecular dynamics. J Comput Aided Mol Des 19:329–340. https://doi.org/10.1007/s10822-005-7003-0.
13. Savard P-Y, Gagné SM. 2006. Backbone dynamics of TEM-1 deter-

mined by NMR: evidence for a highly ordered protein. Biochemistry 45:11414–11424. https://doi.org/10.1021/bi060414q.
14. Doucet N, Savard P-Y, Pelletier JN, Gagné SM. 2007. NMR investigation of Tyr105 mutants in TEM-1 beta-lactamase: dynamics are correlated with function. J Biol Chem 282:21448–21459. https://doi.org/10.1074/jbc.M609777200.
15. Morin S, Gagné SM. 2009. NMR dynamics of PSE-4 β-lactamase: an interplay of ps-ns order and μs-ms motions in the active site. Biophys J 96:4681–4691. https://doi.org/10.1016/j.bpj.2009.02.068.
16. Fisette O, Gagné S, Lagüe P. 2012. Molecular Dynamics of Class A β-lactamases—Effects of Substrate Binding. Biophys J 103:1790–1801. https://doi.org/10.1016/j.bpj.2012.09.009.
17. Risso VA, Gavira JA, Mejia-Carmona DF, Gaucher EA, Sanchez-Ruiz JM. 2013. Hyperstability and substrate promiscuity in laboratory resurrections of precambrian β-lactamases. J Am Chem Soc 135:2899–2902. https://doi.org/10.1021/ja311630a.
18. Zou T, Risso VA, Gavira JA, Sanchez-Ruiz JM, Ozkan SB. 2015. Evolution of conformational dynamics determines the conversion of a promiscuous generalist into a specialist enzyme. Mol Biol Evol 32:132–143. https://doi.org/10.1093/molbev/msu281.
19. Risso VA, Martinez-Rodriguez S, Candel AM, Krüger DM, Pantoja-Uceda D, Ortega-Muñoz M, Santoyo-Gonzalez F, Gaucher EA, Kamerlin SCL, Bruix M, Gavira JA, Sanchez-Ruiz JM. 2017. De novo active sites for resurrected Precambrian enzymes. Nat Commun 8:16113. https://doi.org/10.1038/ncomms16113.
20. Clouthier CM, Morin S, Gobeil SMC, Doucet N, Blanchet J, Nguyen E, Gagné SM, Pelletier JN. 2012. Chimeric β-lactamases: global conservation of parental function and fast time-scale dynamics with increased slow motions. PLoS One 7:e52283. https://doi.org/10.1371/journal.pone.0052283.
21. Gobeil SMC, Clouthier CM, Park J, Gagné D, Berghuis AM, Doucet N, Pelletier JN. 2014. Maintenance of native-like protein dynamics may not be required for engineering functional proteins. Chem Biol 21:1330–1340. https://doi.org/10.1016/j.chembiol.2014.07.016.
22. González MM, Abriata LA, Tomatis PE, Vila AJ. 2016. Optimization of conformational dynamics in an epistatic evolutionary trajectory. Mol Biol Evol 33:1768–1776. https://doi.org/10.1093/molbev/msw052.
23. Meroueh SO, Fisher JF, Schlegel HB, Mobashery S. 2005. Ab initio QM/MM study of class A β-lactamase acylation: dual participation of Glu166 and Lys73 in a concerted base promotion of Ser70. J Am Chem Soc 127:15397–15407. https://doi.org/10.1021/ja051592u.
24. Vandavasi VG, Weiss KL, Cooper JB, Erskine PT, Tomanicek SJ, Ostermann A, Schrader TE, Ginell SL, Coates L. 2016. Exploring the mechanism of β-lactam ring protonation in the class A β-lactamase acylation mechanism using neutron and X-ray crystallography. J Med Chem 59:474–479. https://doi.org/10.1021/acs.jmedchem.5b01215.
25. Drawz SM, Bonomo RA. 2010. Three decades of β-lactamase inhibitors. Clin Microbiol Rev 23:160–201. https://doi.org/10.1128/CMR.00037-09.
26. Papp-Wallace KM, Bonomo RA. 2016. New β-lactamase inhibitors in the clinic. Infect Dis Clin North Am 30:441–464. https://doi.org/10.1016/j.idc.2016.02.007.
27. Tehrani K, Martin NI. 2018. β-lactam/β-lactamase inhibitor combinations: an update. Medchemcomm 9:1439–1456. https://doi.org/10.1039/c8md00342d.
28. Kurz SG, Bonomo RA. 2012. Reappraising the use of β-lactams to treat tuberculosis. Expert Rev Anti Infect Ther 10:999–1006. https://doi.org/10.1586/eri.12.96.
29. Watkins RR, Papp-Wallace KM, Drawz SM, Bonomo RA. 2013. Novel β-lactamase inhibitors: a therapeutic hope against the scourge of multidrug resistance. Front Microbiol 4:392. https://doi.org/10.3389/fmicb.2013.00392.
30. Drawz SM, Papp-Wallace KM, Bonomo RA. 2014. New β-lactamase inhibitors: a therapeutic renaissance in an MDR world. Antimicrob Agents Chemother 58:1835–1846. https://doi.org/10.1128/AAC.00826-13.
31. Elings W, Tassoni R, van der Schoot SA, Luu W, Kynast JP, Dai L, Blok AJ, Timmer M, Florea BI, Pannu NS, Ubbink M. 2017. Phosphate promotes the recovery of *Mycobacterium tuberculosis* β-lactamase from clavulanic acid inhibition. Biochemistry 56:6257–6267. https://doi.org/10.1021/acs.biochem.7b00556.
32. Soroka D, Ourghanlian C, Compain F, Fichini M, Dubée V, Mainardi JL, Hugonnet JE, Arthur M. 2017. Inhibition of β-lactamases of mycobacteria by avibactam and clavulanate. J Antimicrob Chemother 72:1081–1088. https://doi.org/10.1093/jac/dkw546.
33. García de la Torre J, Huertas ML, Carrasco B. 2000. HYDRONMR: prediction of NMR relaxation of globular proteins from atomic-level structures and hydrodynamic calculations. J Magn Reson 147:138–146. https://doi.org/10.1006/jmre.2000.2170.
34. Xu H, Hazra S, Blanchard JS. 2012. NXL104 irreversibly inhibits the β-lactamase from *Mycobacterium tuberculosis*. Biochemistry 51:4551–4557. https://doi.org/10.1021/bi300508r.
35. Waudby CA, Ramos A, Cabrita LD, Christodoulou J. 2016. Two-dimensional NMR lineshape analysis. Sci Rep 6:24826. https://doi.org/10.1038/srep24826.
36. Hugonnet J-E, Blanchard JS. 2007. Irreversible inhibition of the *Mycobacterium tuberculosis* beta-lactamase by clavulanate. Biochemistry 46:11998–12004. https://doi.org/10.1021/bi701506h.
37. Stivers JT, Abeygunawardana C, Mildvan AS, Whitman CP. 1996. ^{15}N NMR relaxation studies of free and inhibitor-bound 4-oxalocrotonate tautomerase: backbone dynamics and entropy changes of an enzyme upon inhibitor binding. Biochemistry 35:16036–16047. https://doi.org/10.1021/bi961834q.
38. Tassoni R, Blok A, Pannu NS, Ubbink M. 2019. New conformations of acylation adducts of inhibitors of β-lactamase from Mycobacterium tuberculosis. Biochemistry 58:997–1009. https://doi.org/10.1021/acs.biochem.8b01085.
39. Lecoq L, Bougault C, Hugonnet JE, Veckerlé C, Pessey O, Arthur M, Simorre JP. 2012. Dynamics induced by β-lactam antibiotics in the active site of Bacillus subtilis L,D-transpeptidase. Structure 20:850–861. https://doi.org/10.1016/j.str.2012.03.015.
40. Frederick TE, Peng JW. 2018. A gratuitous β-Lactamase inducer uncovers hidden active site dynamics of the Staphylococcus aureus BlaR1 sensor domain. PLoS One 13:e0197241. https://doi.org/10.1371/journal.pone.0197241.
41. Sagar A, Haleem N, Bashir YM, Ashish. 2017. Search for non-lactam inhibitors of Mtb β-lactamase led to its open shape in apo state: new concept for antibiotic design. Sci Rep 7:6204. https://doi.org/10.1038/s41598-017-06023-3.
42. Olmos JL, Pandey S, Martin-Garcia JM, Calvey G, Katz A, Knoska J, Kupitz C, Hunter MS, Liang M, Oberthuer D, Yefanov O, Wiedorn M, Heyman M, Holl M, Pande K, Barty A, Miller MD, Stern S, Roy-Chowdhury S, Coe J, Nagaratnam N, Zook J, Verburgt J, Norwood T, Poudyal I, Xu D, Koglin J, Seaberg MH, Zhao Y, Bajt S, Grant T, Mariani V, Nelson G, Subramanian G, Bae E, Fromme R, Fung R, Schwander P, Frank M, White TA, Weierstall U, Zatsepin N, Spence J, Fromme P, Chapman HN, Pollack L, Tremblay L, Ourmazd A, Phillips GN, Schmidt M. 2018. Enzyme intermediates captured "on the fly" by mix-and-inject serial crystallography. BMC Biol 16:59. https://doi.org/10.1186/s12915-018-0524-5.
43. Golemi-Kotra D, Meroueh SO, Kim C, Vakulenko SB, Bulychev A, Stemmler AJ, Stemmler TL, Mobashery S. 2004. The importance of a critical protonation state and the fate of the catalytic steps in class A beta-lactamases and penicillin-binding proteins. J Biol Chem 279:34665–34673. https://doi.org/10.1074/jbc.M313143200.
44. Nichols DA, Hargis JC, Sanishvili R, Jaishankar P, Defrees K, Smith EW, Wang KK, Prati F, Renslo AR, Woodcock HL, Chen Y. 2015. Ligand-induced proton transfer and low-barrier hydrogen bond revealed by X-ray crystallography. J Am Chem Soc 137:8086–8095. https://doi.org/10.1021/jacs.5b00749.
45. Pan X, He Y, Lei J, Huang X, Zhao Y. 2017. Crystallographic snapshots of class A β-lactamase catalysis reveal structural changes that facilitate β-lactam hydrolysis. J Biol Chem 292:4022–4033. https://doi.org/10.1074/jbc.M116.764340.
46. Vandavasi VG, Langan PS, Weiss KL, Parks JM, Cooper JB, Ginell SL, Coates L. 2017. Active-site protonation states in an acyl-enzyme intermediate of a class A β-lactamase with a monobactam substrate. Antimicrob Agents Chemother 61:e01636-16. https://doi.org/10.1128/AAC.01636-16.
47. Langan PS, Vandavasi VG, Cooper SJ, Weiss KL, Ginell SL, Parks JM, Coates L. 2018. Substrate binding induces conformational changes in a class A β-lactamase that prime it for catalysis. ACS Catal 8:2428–2437. https://doi.org/10.1021/acscatal.7b04114.
48. Tomanicek SJ, Blakeley MP, Cooper J, Chen Y, Afonine PV, Coates L. 2010. Neutron diffraction studies of a class A β-lactamase Toho-1 E166A/R274N/R276N triple mutant. J Mol Biol 396:1070–1080. https://doi.org/10.1016/j.jmb.2009.12.036.
49. Ibuka AS, Ishii Y, Galleni M, Ishiguro M, Yamaguch K, Frère J-M, Matsuzawa H, Sakai H. 2003. Crystal structure of extended-spectrum β-lactamase Toho-1: insights into the molecular mechanism for catalytic reaction and substrate specificity expansion. Biochemistry 42:10634–10643. https://doi.org/10.1021/bi0342822.

50. Ambler RP, Coulson AFW, Frère JM, Ghuysen JM, Joris B, Forsman M, Levesque RC, Tiraby G, Waley SG. 1991. A standard numbering scheme for the class A beta-lactamases. Biochem J 276:269–272. https://doi.org/10.1042/bj2760269.
51. Pervushin K, Riek R, Wider G, Wüthrich K. 1997. Attenuated T2 relaxation by mutual cancellation of dipole-dipole coupling and chemical shift anisotropy indicates an avenue to NMR structures of very large biological macromolecules in solution. Proc Natl Acad Sci U S A 94:12366–12371. https://doi.org/10.1073/pnas.94.23.12366.
52. Schanda P, Van Melckebeke H, Brutscher B. 2006. Speeding up three-dimensional protein NMR experiments to a few minutes. J Am Chem Soc 128:9042–9043. https://doi.org/10.1021/ja062025p.
53. Vranken WF, Boucher W, Stevens TJ, Fogh RH, Pajon A, Llinas M, Ulrich EL, Markley JL, Ionides J, Laue ED. 2005. The CCPN data model for NMR spectroscopy: development of a software pipeline. Proteins 59:687–696. https://doi.org/10.1002/prot.20449.
54. Bae S-H, Dyson HJ, Wright PE. 2009. Prediction of the rotational tumbling time for proteins with disordered segments. J Am Chem Soc 131:6814–6821. https://doi.org/10.1021/ja809687r.
55. Bruker Corporation. 2017. Dynamics Center. User manual, version 002. Bruker, Rheinstetten, Germany.
56. Woessner DE. 1962. nuclear spin relaxation in ellipsoids undergoing rotational brownian motion. J Chem Phys 37:647–654. https://doi.org/10.1063/1.1701390.
57. Vallurupalli P, Hansen DF, Stollar E, Meirovitch E, Kay LE. 2007. Measurement of bond vector orientations in invisible excited states of proteins. Proc Natl Acad Sci U S A 104:18473–18477. https://doi.org/10.1073/pnas.0708296104.
58. Delaglio F, Grzesiek S, Vuister G, Zhu G, Pfeifer J, Bax A. 1995. NMRPipe: a multidimensional spectral processing system based on UNIX pipes. J Biomol NMR 6:277–293. https://doi.org/10.1007/bf00197809.
59. Hansen DF, Yang D, Feng H, Zhou Z, Wiesner S, Bai Y, Kay LE. 2007. An exchange-free measure of ^{15}N transverse relaxation: an NMR spectroscopy application to the study of a folding intermediate with pervasive chemical exchange. J Am Chem Soc 129:11468–11479. https://doi.org/10.1021/ja072717t.
60. Hansen DF, Vallurupalli P, Lundström P, Neudecker P, Kay LE. 2008. Probing chemical shifts of invisible states of proteins with relaxation dispersion NMR spectroscopy: how well can we do? J Am Chem Soc 130:2667–2675. https://doi.org/10.1021/ja078337p.
61. Tremblay LW, Hugonnet J-E, Blanchard JS. 2008. Structure of the covalent adduct formed between *Mycobacterium tuberculosis* beta-lactamase and clavulanate. Biochemistry 47:5312–5316. https://doi.org/10.1021/bi8001055.